Optical oscillator strengths of noble-gas resonance transitions in the vacuum-ultraviolet region

R. C. G. Ligtenberg, P. J. M. van der Burgt,* S. P. Renwick, W. B. Westerveld,† and J. S. Risley
Atomic Collisions Laboratory, Department of Physics, North Carolina State University, Raleigh, North Carolina 27695-8202
(Received 28 May 1993; revised manuscript received 3 December 1993)

We report the results of an accurate measurement of the optical oscillator strengths of the prominent resonance lines of He, Ne, Ar, and Kr in the vacuum-ultraviolet region based on the absorption of resonance radiation. The transmission of this radiation through a layer of gas of finite thickness is measured as a function of the number density of the gas. The transmission function is fitted to this data to obtain the absorption oscillator strength. The accuracy of the present measurements ranges from 2.5% to 4%. The results are as follows: He I (58.4 nm), 0.2683±0.0075 (2.8%); He I (5.37 nm), 0.0717±0.0024 (3.4%); Ne I (74.4 nm), 0.010 17±0.000 30 (2.9%); Ne I (73.6 nm), 0.1369±0.0035 (2.6%); Ar I (106.7 nm), 0.0616±0.0021 (3.4%); Ar I (104.8 nm), 0.2297±0.0093 (4.0%); Kr I (123.6 nm), 0.1751±0.0049 (2.8%); Kr I (116.5 nm), 0.1496±0.0038 (2.5%).

PACS number(s): 32.70.Cs, 35.80.+s

I. INTRODUCTION

We present the results of a measurement of the optical oscillator strengths for the transitions from the ground state to the first two excited states of the noble-gas atoms helium, neon, argon, and krypton. Accurately measured oscillator strengths provide benchmarks for theoretical calculations, as well as data for applications in plasma physics, the atmospheric sciences, and astrophysics.

We measure atomic absorption oscillator strengths by making use of the absorption of resonance radiation by atoms in the gas phase. The experimental setup is shown in Fig. 1. The electron gun in a static gas cell produces a well-collimated beam of electrons. Gas atoms in the electron beam emit characteristic line radiation upon decay after they have been collisionally excited by the energetic electrons. The lifetimes of the excited states observed in this work are sufficiently short that the excited atoms decay before they leave the electron beam. The electron beam source of radiation is hereafter referred to as the electron-atom source [1,2]. A detector consisting of a spectrometer and a photomultiplier collects radiation emitted at right angles to the electron beam.

The gas atoms in the cell readily absorb the resonance radiation emitted by the electron-atom source. The degree of absorption depends on the density and the absorption coefficient of the gas and the distance the radiation travels through the gas. In this work the fraction $T_R(n)$ of the light transmitted through the layer of gas is measured as a function of the gas number density n. The absorption oscillator strength of the transition is obtained from an analysis of this data.

II. TRANSMISSION OF RESONANCE RADIATION

The absorption coefficient $a(\nu)$ of the gas for a resonance line is defined by [3]

$$I(\nu,x)=I(\nu,0)e^{-a(\nu)x}, \quad (1)$$

where ν is the frequency of the absorbed light, $I(\nu,x)$ is the intensity of the resonance line in the beam at a distance x from the electron-atom source, and $I(\nu,0)$ is the intensity of the radiation at the source. The absorption coefficient is, in general, frequency dependent.

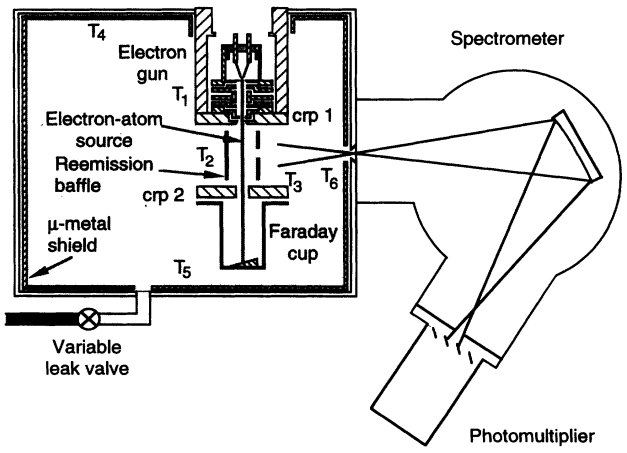

FIG. 1. General overview of the experimental apparatus. The electron beam produced by the electron gun is immersed in the gas and forms the electron-atom source of radiation. An aluminum reemission baffle is inserted between the electron gun and Faraday cup. Light emitted in the direction of the spectrometer is wavelength selected and then detected by the photomultiplier. The μ-metal shield minimizes the penetration of external magnetic fields into the cell. The target gas pressure is regulated with the variable leak valve. The locations of the temperature probes are indicated by T_1 through T_6.

*Present address: Department of Physics, University of Windsor, Windsor, Ontario, Canada N9B 3P4.
†Permanent address: Department of Physics, University of Utrecht, 3584 CC Utrecht, The Netherlands.

For a purely Doppler broadened line the absorption coefficient $a(\nu)$ is given by [3,4]

$$a(\nu)=a_0 \exp\left[-\frac{Mc^2}{2kT}\left[\frac{\nu}{\nu_0}-1\right]^2\right], \quad (2)$$

where ν_0 is the central line frequency of the resonant transition, M is the atomic mass of the gas, c is the speed of light, k is Boltzmann's constant, and T is the absolute temperature of the gas. Pressure broadening does not contribute to the widths of the line shape under the conditions encountered in the present measurements. The quantity a_0 is given by

$$a_0=\frac{e^2}{4\pi\varepsilon_0 mc}\left[\frac{\pi M}{2kT}\right]^{1/2}\lambda_0 f n , \quad (3)$$

where e is the electron charge, m is the mass of the electron, ε_0 is the vacuum permittivity, λ_0 is the wavelength of the resonant transition, n is the density of the gas, and f is the absorption oscillator strength for the transition. The total intensity $I(x)$ of a resonance line at a distance x from the electron-atom source is given by the integral over the line profile $I(\nu,x)$:

$$I(x)=\int_0^\infty I(\nu,x)d\nu=\int_0^\infty I(\nu,0)e^{-a(\nu)x}d\nu . \quad (4)$$

In the absence of recoil effects in the excitation process, the emission profile $I(\nu,0)$ of the light from the electron-atom source has the same Gaussian shape, due to the Maxwellian atomic velocity distribution, as does the absorption coefficient in Eq. (2). It is given by

$$I(\nu,0)=I(\nu_0,0)\exp\left[-\frac{Mc^2}{2kT}\left[\frac{\nu}{\nu_0}-1\right]^2\right], \quad (5)$$

where $I(\nu_0,0)$ is the intensity at the central frequency ν_0 of the source at position $x=0$.

The transmission function $T_R(a_0x)$ is defined as the ratio at the total intensity $I(x)$ of a resonance line at a distance x from the electron-atom source to the total initial intensity $I(0)$:

$$T_R(a_0x)=\frac{I(x)}{I(0)}=\frac{\int_0^\infty I(\nu,0)e^{-a(\nu)x}d\nu}{\int_0^\infty I(\nu,0)d\nu} . \quad (6)$$

It is convenient to express the transmission as a function of the parameter a_0x [3,4] where a_0 contains the dependence on the gas number density n. The absorption and emission profiles are identical when Doppler broadening is the dominant contributor to the line shape. Under these circumstances Eq. (6) for the transmission function can be expanded into a power series [3] as

$$T_r(a_0x)=\sum_{n=0}^{\infty}\frac{(-a_0x)^n}{n!\sqrt{n+1}} . \quad (7)$$

With this expansion the transmission can be calculated to an arbitrary precision for values of the parameter a_0x smaller than about 10. The exponential approximation [4]

$$T_r(a_0x)\approx \exp\left[\frac{-a_0x}{\sqrt{2}}\right], \quad (8)$$

is not accurate enough for this work.

The emission profile of a spectral line from the electron-atom source is affected by the recoil of the atom after the scattering of an exciting electron; however, Westerveld and co-workers [4,5] have shown that at room temperature the recoil velocity imparted onto the gas atoms is small compared to their average kinetic velocity and that the correction to the value of the measured oscillator strength is much less than 1%.

The emission and absorption profiles are also affected by the isotropic abundance of Ne and Kr. If there is no overlap, the line shapes of two different isotopes of an atom propagate independently through the gas with each line experiencing a different absorption coefficient which depends on the partial density of the corresponding isotope. Westerveld and co-workers [4,5] found that for Ne the isotope shifts are small compared to the Doppler widths and that these small shifts have no effect on the transmission measurements. Measurements by Turner [6] indicate that the same is true for the Kr resonance lines.

III. APPARATUS

The clean ultrahigh-vacuum apparatus consists of a gas cell containing the electron-atom source of radiation, and the spectrometer photomultiplier. The gas pressure is measured with an ionization gauge tube which is calibrated *in situ* against a spinning rotor friction gauge. The electron beam current is collected in a Faraday cup. A measurement consists of recording, in a range of gas pressures, the photomultiplier count rate, the electron beam current, and the ionization gauge signal. For each pressure, these three signals are recorded simultaneously in three accumulators, along with the time duration of the run by a microcomputer. During a measurement, the temperature of the gas is also recorded as is the base pressure in the cell.

A. Gas cell

The gas cell consists of a cylindrical stainless steel vacuum chamber, 25 cm long and 15 cm in diameter. It contains the electron-gun–Faraday-cup assembly as shown in Fig. 1. After evacuation to a base pressure of 10^{-7} Torr, the target gas is fed into the cell through a variable leak valve to the desired pressure. The beam of electrons produced by the electron gun travels through the gas in the collision region over a distance of 4 cm to the Faraday cup. A μ-metal shield lining the inside wall of the gas cell reduces the magnetic field in the central region of the cell to about 5 mG. The metal plates that bound the collision region plate nos. 1 and 2 (crp1 and crp2) are held at ground potential.

A radiation baffle in the form of an aluminum cylinder with a diameter of 1.5 cm is mounted concentric with the electron-atom source and is electrically grounded. Radiation from the electron-atom source is absorbed at the walls of the baffle and does not illuminate the gas in the

gas cell. A small slot in the baffle allows only a narrow beam of radiation to pass to the detector. The radiation baffle effectively eliminates the contribution to the detector signal from the reemission of resonance radiation that would otherwise be absorbed throughout the gas cell.

The gas cell is equipped with three pressure measuring devices. A Varian model 564 broad range ionization gauge tube is used to measure the target gas pressure during the data accumulation cycles. An MKS model 2 spinning rotor gauge (SRG) with an absolute accuracy of 1.5% is used to calibrate the ion gauge. An MKS Baratron 310 capacitance manometer is used to transfer the known calibration of the SRG for one gas to a gas for which the calibration factor of the SRG is not known.

To maintain a high-quality, hydrocarbon-free vacuum, a Varian VK-12A cryopump with a pumping speed of 1000 l/s for air is used for the main system to produce a 5×10^{-9} Torr vacuum in the spectrometer. An auxiliary Leybold Heraeus TMP-360 turbo pump with a pumping speed of 350 l/s is used to pump He. The gas cell is also pumped by a 50 l/s SEAS GP50 getter pump to reduce non-noble-gas contamination. The base pressure in the gas cell is 1×10^{-7} Torr.

High-purity target gas is fed into the gas cell through a Granville Phillips model 203 variable leak valve. The gas delivery system allows the gas to be fed either into the gas cell or into the high vacuum pump while bypassing the gas cell. The latter mode is used to measure the background pressure in the gas cell without disturbing the setting of the variable leak valve. This is necessary for measurements at very low target gas pressures where a low photon count rate necessitates an extended accumulation time, sometimes over 24 h. Under these circumstances the fluctuations in the background pressure caused by variations in the room temperature must be carefully measured.

B. Electron gun

The electron gun, a scaled down version of a design by Erdman and Zipf [2,7], uses a hot filament with electrostatic extraction and focusing plates. It produces a collimated beam of electrons with an energy between 50 and 1000 eV. The diameter of the beam is about 1 mm. The tungsten ribbon filament is premounted on a ceramic base inside a Wehnelt cap. The electron gun is housed inside a copper heat shield which is in thermal contact with the electron-gun holder. Cooling water circulating through a duct in the holder removes the heat generated by the filament. During operation of the electron gun the temperature of the shield is about 300 K (T_1 in Fig. 1) and depends slightly on the temperature of the cooling water. The temperature of the wall of the gas cell rises from 297 to 303 K (T_4 and T_5 in Fig. 1) when the gun is turned on. The enclosure provided by the heat shield is differentially pumped to prevent any gas that has entered the enclosure from flowing back into the gas cell.

The electrons extracted from the filament are accelerated through an electrostatic Einzel lens with adjustable potentials for focusing. The 100-μA beam of electrons passes through crp1 into the field-free interaction region. After passing through the interaction region the beam enters the Faraday cup through crp2. The Faraday cup is biased at a voltage of +50 V with respect to the field-free region to prevent the escape of secondary electrons from the cup. The current collected in the Faraday cup, measured with an accuracy of 0.3%, is fed to an accumulator which is read out by the microcomputer. The two plates crp1 and crp2 are individually connected to ground potential through a current meter to register any deposited electrons. The current on the plates is less than 0.5% of the current that is collected in the Faraday cup.

C. Detection system

A Minuteman 302 VM spectrometer based on a modified Seya-Namioka design [8,9] is used to disperse the radiation. It utilizes a Jobin-Yvon 1200-groove/mm, MgF_2-overcoated, aberration-corrected, concave holographic grating with a dispersion of 40 Å/mm. The fixed width of the entrance slit is 0.07 mm and the height is 10 mm. The width of the bilateral exit slit, with a height of 4 mm, can be externally adjusted with a micrometer. The instrumental full width at half maximum (FWHM) is 3.5 Å when the exit slit width is set equal to the entrance slit width. For wavelength selection the grating is rotated by a stepper motor where an advancement of 160 steps of the stepper motor corresponds to a 1-Å change.

An EMI model 9642/3A venetian-blind photomultiplier tube with a BeCu cathode is used to measure the intensity of the dispersed radiation. A plate located in front of the cathode is biased at +50 V to prevent the loss of backscattered electrons [10]. The original dynode resistor chain with a total resistance of 36 MΩ was replaced by a set with a total resistance of 3.6 MΩ to increase the resistor current thereby keeping the photomultiplier at a higher temperature for better degassing. This improves the long-term stability of the photomultiplier detection efficiency [11]. The anode signal is fed into the pulse counting system.

D. Automation

The data collection is automated with a microcomputer controlling the process, see Fig. 2. Using a custom interface, pulses representing the photon counts, the electron beam current, and the gas pressure are accumulated simultaneously in three accumulators. The run time is also recorded. After the leak value is adjusted to admit the target gas into the gas cell at the desired pressure, a computer program is used to accumulate the signals and to sample the base pressure during the run by periodically switching the gas routing from the gas cell to the high vacuum pump.

IV. MEASUREMENT PROCEDURE

The measurement method involves measuring the transmission $T_R(a_0x)$ of the resonance line through a layer of gas of constant thickness for a range of gas pressures. The distance over which the transmission takes

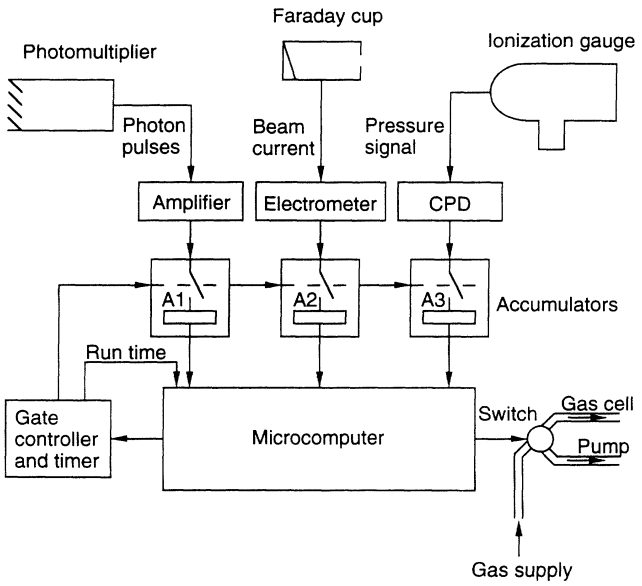

FIG. 2. Signal flow diagram showing the simultaneous accumulation of the photomultiplier pulses (A1), the beam current pulses (A2), and the pressure pulses (A3) by the computer program. For the measurement of the background signals the gas supply is switched from the gas cell to the high vacuum pump.

place is fixed. The quantities that have to be measured at each pressure are the detector count rate, the electron beam current, the target gas pressure, and the gas temperature.

A. Spectrometer setting

A wavelength scan over the line of interest is used to find the setting of the spectrometer for the peak of the instrumental line shape and to determine whether there is any overlap from neighboring lines. From scans at different widths of the exit slit the optimal width for the exit slit is chosen to allow complete collection of the spectral line at the photomultiplier.

B. Detector count rate

The photomultipler detects the fraction T_R of the radiation emitted by the electron-atom source that is transmitted through the absorbing layer of gas between the source and the entrance slit to the spectrometer. The total rate of production I of photons of frequency ν along a section of length l of the electron-atom source is given by

$$I=i_e n l \sigma \ , \tag{9}$$

where i_e is the number of electrons in the electron beam per second, l is the length of the beam viewed, and σ is the electron impact photoemission cross section for the transition. The emission cross section σ includes the cascade contributions from higher excited states.

In the absence of absorption, a constant fraction ε of the emitted radiation is recorded by the detector, where ε is determined by the angular distribution of the emitted radiation, the collection solid angle of the detector, and the quantum efficiency of the detector. If the observed radiation comes from a resonance transition then the detected intensity is further reduced by absorption in the gas to a fraction εT_R. The photon count rate $c(n)$ at a gas density n is

$$c(n)=\varepsilon T_R(a_0 x) I \ . \tag{10}$$

Note that the transmission $T_R(a_0 x)$ is proportional to the photon count rate $c(n)$.

C. Target gas pressure

The target gas pressure is measured with an ionization gauge tube which is calibrated against a spinning rotor gauge. The ionization gauge is linear from 10^{-2} down to 10^{-10} Torr (x-ray limit). The linearity of the gauge was verified between 10^{-3} and 5×10^{-7} Torr by measuring the detector count rate for a nonresonance line as a function of the ionization gauge signal. Additionally, the ionization gauge calibration against the SRG is repeated for each pressure at which the transmission is measured and these data also verify the linearity of the ionization gauge. The collector current from the ionization gauge is converted to a count rate by a Red Nun 8111 charge pump digitizer (CPD). The pulses from the CPD are counted in one of the three accumulators. To relate the registered count rate back to an absolute pressure, the ionization gauge-CPD system is calibrated against a spinning rotor gauge which measures gas pressures with an absolute accuracy of 1.5% down to 1×10^{-6} Torr [12]. The calibration procedure gives an ionization gauge calibration factor k, which is the CPD count rate divided by the gas pressure as indicated by the SRG in counts per second per Torr.

The SRG measures the drag that the surrounding gas exerts on a rotor ball which is magnetically suspended and freely rotating in a thimble that is open to the gas cell. Since the deceleration of the rotor depends on the molecular mass of the gas, an accommodation coefficient of the rotor ball must be entered in the controller. The rotor used in this work was calibrated for He and N_2 to an absolute accuracy of 1.5% at the Pressure and Temperature Division at the National Institute of Standards and Technology (NIST) in Gaithersburg, MD [13]. A Baratron 310 capacitance manometer is used as a transfer standard to determine the accommodation coefficient of the rotor for a gas other than He or N_2. The added uncertainty in the accommodation coefficient due to this transfer standard technique ranges from 0.26% to 0.31%. The accommodation coefficients for the gases used in this experiment are listed in Table I. The total uncertainty in the accommodation coefficient of the SRG rotor for Ne, Ar, and Kr is determined by summing in quadrature the absolute uncertainty (1.5%) in the NIST primary pressure standard and the uncertainty from the transfer process.

Because the offset in the SRG exhibits a slow drift of several μTorr per hour, caused by the thermal expansion of the rotor during spin up, the ionization gauge is used

TABLE I. Accommodation coefficient of the SRG rotor for different gases.

Gas	Accommodation coefficient
He	1.099 (±1.5%)[a]
N_2	1.069 (±1.5%)[a]
Ne	1.058 (±1.53%)
Ar	1.080 (±1.53%)
Kr	1.080 (±1.53%)
Xe	1.103 (±1.53%)

[a]Absolute uncertainty, calibrated at the National Institute of Standards and Technology, Gaithersburg, MD [13].

to record variations in the pressure during data accumulation.

D. Temperature

Six solid-state Analog Devices ADLF 590 temperature probes (labeled T_1 through T_6 in Fig. 1), mounted onto various surfaces inside the gas cell, measure the temperature of the gas. One probe is mounted on the electron-gun housing (T_1), one is mounted onto the radiation baffle surrounding the electron beam (T_2), and the third is mounted onto crp2 (T_3). Two probes are mounted on the μ-metal sheet lining the inside wall of the gas cell, one near the ionization gauge tube (T_4) and one of the opposite side of the cell (T_5). The last probe is mounted near the entrance slit to the spectrometer (T_6). The probe temperatures are equal to the room temperature to within 1 K when no power is applied to the electron gun or to the ionization gauge. During operation, the electron gun and the ionization gauge cause some heating in the gas cell. Figure 3 shows the range of temperatures in the gas cell for two situations; (a) when the electron gun and the ionization gauge are off and the whole cell is in equilibrium at room temperature and (b) when a steady temperature gradient has established itself throughout the cell after the electron gun and the ionization gauge have been turned on. The graph shows that the probe temperatures increase from 4 to 7 K due to the operation of the electron gun and the ionization gauge. The temperature of probe T_1 on the copper jacket of the electron gun is the lowest as a consequence of its close placement to the cooling water duct. The temperature of probe T_2 on the radiation baffle around the electron beam is taken to measure the temperature of the gas most accurately because of its proximity to the interacting region.

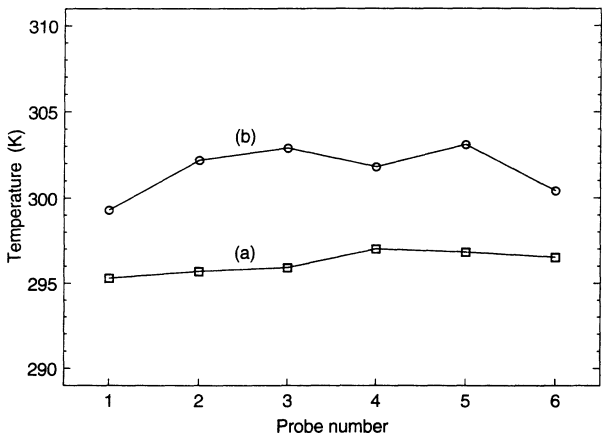

FIG. 3. Reading of the temperature probes T_1 through T_6 in the gas cell. (a) The electron gun and the ionization gauge are off and the entire gas cell is in equilibrium at room temperature. (b) Steady-state temperatures after the electron gun and the ionization gauge have been running for over 24 h. The locations of the probes are (see Fig. 1) T_1, electron-gun housing; T_2, reemission baffle; T_3, collision region plate no. 2; T_4, μ-metal shield (ionization gauge side); T_5, μ-metal shield (Baratron side); and T_6, spectrometer entrance slit.

E. Transmission

From Eqs. (9) and (10), and the ideal gas law $p=nkT$, the measured transmission $T_R(a_0x)$ is given by

$$AT_R(a_0x)=\frac{c(p)}{i_eP}\ , \tag{11}$$

where $c(p)$ is the photon count rate as a function of the pressure p. The factor A is a constant and may be chosen to be unity at zero pressure. With this choice the transmission is obtained as a fraction ranging from zero (no transmission) to unity (100% transmission).

F. Data accumulation

The primary quantities to be measured at a given gas pressure are the photon count rate c, the target gas pressure p, the electron beam current i_e, and the gas temperature T. Small fluctuations in the pressure and the beam current are accounted for by integrating these signals over the run time. The accumulation time t at each target gas pressure is chosen such that a total of at least 15 000 photons are detected to keep counting statistics below 1%. This leads to an accumulation time from 20 min at the higher pressures ($>10^{-4}$ Torr) to up to 24 h at the lowest pressures ($<10^{-6}$ Torr). A single run is divided into about ten or more shorter periods for which the accumulated counts are recorded separately to expose any unusual fluctuations or unexpected drifts in the recorded count rates.

The background count rate of the photomultiplier and the residual gas pressure in the cell are obtained from a run during which no target gas is admitted into the cell. The background signals are subtracted from the respective total signals.

G. Data analysis

The pressure p of the gas is computed from

$$p=\frac{(P/t)-(P'/t')}{k}\ , \tag{12}$$

where P is the number of accumulated pressure counts in time t and P' is the accumulated number of background pressure counts in time t'. The factor k is the ionization gauge calibration constant defined in Sec. IV C. The nor-

malized photomultiplier count rate $N(p)$ is computed as

$$N(p)=\frac{(C/t)-(C'/t')}{(I/t)p} , \tag{13}$$

where c and C' are the accumulated photomultiplier counts in times t and t', respectively, and I represents the accumulated current counts in time t.

Comparing Eqs. (11) and (13) shows that the normalized photomultiplier count rate $N(p)$ is proportional to the transmission

$$N(p)=A_1 T_R(a_0 x) . \tag{14}$$

The numerical value of the scaling factor A_1 is not relevant to the determination of the oscillator strength.

The transmission function $T_R(a_0 x)$, defined in Eq. (6) and adapted for numerical evaluation in Eq. (7), is fitted to the normalized photomultiplier count rate N as a function of the pressure p with a weighted least-squares fitting routine containing two fitting parameters A_1 and A_2. The uncertainties in $N(p)$ are used as the weight factors in the fit. The two fitting parameters are defined as

$$A_1 T_R(A_2 p)=A_1 \sum_{n=0}^{M} \frac{(-A_2 p)^n}{n!\sqrt{n+1}} . \tag{15}$$

Eighteen terms of the series expansion Eq. (15) are included in the fitting function, allowing a maximum error in the evaluation of the transmission, for transmissions larger than 0.2, of 1 part in 10^8.

The parameter A_2 is given by

$$A_2=\frac{a_0 x}{p} , \tag{16}$$

where a_0 is given in Eq. (3). Since the distance x and the gas temperature T are measured directly, the oscillator strength f is determined from the fitted value of the parameter A_2:

$$f=\frac{4\pi\varepsilon_0 mc}{e^2}\left[\frac{2k^3}{\pi M}\right]^{1/2}\frac{1}{\lambda_0}\left[\frac{T^{3/2}}{x}\right]A_2 . \tag{17}$$

V. ERROR ANALYSIS

The experimental uncertainty Δf in the oscillator strength is found by propagating through in Eq. (17) the uncertainties in the measured values of the temperature T, the transmission distance x, and the uncertainty in the fitted value of the free parameter A_2. This gives the following sum in quadrature for the relative uncertainties:

$$\frac{\Delta f}{f}=\left[\left[\frac{3}{2}\frac{\Delta T}{T}\right]^2+\left[\frac{\Delta x}{x}\right]^2+\left[\frac{\Delta A_2}{A_2}\right]^2\right]^{1/2} . \tag{18}$$

A. Uncertainty in the temperature

A measurement with two sample temperature probes in a bath containing a mixture of ice and water confirmed the manufacturer's stated absolute accuracy of ± 1 K.

The reading of temperature probe T_2, situated the closest to the collision region and the region through which the radiation passes to the detector, is taken as the relevant temperature T of the gas. The uncertainty ΔT in this temperature is ± 1 K.

B. Uncertainty in the distance

The distance x over which the transmission is measured is the distance from the center line of the electron-atom source to the face of the knife edges which constitute the entrance slit of the spectrometer. The distances are measured with the electron gun mounted in place in the gas cell using a depth gauge and a pair of calipers with a resolution of 0.001 in (0.025 mm). Assuming that the center line of the electron-atom source coincides with the center line of the electron-gun assembly, the distance x was measured to be 42.42 ± 0.29 mm.

Since the electron beam is defined by a set of apertures, the actual path of the beam through the collision region is not known precisely. The maximum displacement of the electron beam from the center line of the electron-gun assembly can be found from the geometry of the defining apertures through which the beam passes, first into the collision region and then into the Faraday cup. These apertures define a cone with a length of 32 mm, a diameter at the base of 3.81 mm, and a diameter at the top of 1.27 mm. Since 99.9% of the beam current passes into the Faraday cup without hitting crp2, it is assumed that the diameter of the beam has a magnitude equal to the diameter of the exit aperture of the electron gun (1.27 mm) and that the displacement of the axis of the beam is no more than 0.6 mm from the center line of the electron-gun assembly. This assumption gives a maximum uncertainty in the position of the electron beam of ± 0.6 mm. The total uncertainty in the transmission distance x is the sum in quadrature of the uncertainty in the distance between the center line of the electron gun and the spectrometer entrance slit (± 0.29 mm) and the uncertainty in the position of the electron beam with respect to the center line of the electron gun (± 0.6 mm) and amounts to ± 0.67 mm, which is 1.57% of the 42.42 mm distance x.

C. Uncertainty in the fitting

The least-squares routine used for the fitting of the transmission function takes into account the uncertainties in the dependent variable (the normalized detector count rate as weighting factors), but not the independent variable (the gas pressure). This procedure is equivalent to assuming that the uncertainty in the independent variable is small in comparison to the uncertainty in the dependent variable. This assumption is justified if we include only the random measurement errors in the uncertainty of the independent variable (the gas pressure). A possible systematic error in the pressure due to the uncertainty in the absolute calibration of the ionization gauge tube is accounted for separately and then added to the uncertainty in the parameter A_2 from the fit. The total uncertainty in the fitted value of the parameter A_2 is given by the sum in quadrature:

$$(\Delta A_2)^2=\sqrt{(\Delta A_{2,\mathrm{fit}})^2+(\Delta A_{2,\mathrm{cal}})^2}\ . \tag{19}$$

The fitting routine returns the fitted values of A_1 and A_2 together with the associated covariance matrix and the χ^2 of the fit. The uncertainty $\Delta A_{2,\mathrm{fit}}$ is obtained from the covariance matrix. $\Delta A_{2,\mathrm{cat}}$ represents the uncertainty in A_2 due to the uncertainty in the absolute calibration of the ionization gauge.

The uncertainty $\Delta A_{2,\mathrm{fit}}$ is a consequence of the scatter in the values of the normalized detector counts N with respect to the shape of the transmission curve and the random uncertainty ΔN in each measurement point $N(p)$. The uncertainty ΔN in the normalized photomultiplier count rate reflects only the random errors in the detector count rate c, the beam current i_e, the beam current i_e, and the gas pressure p. From Eq. (13) we get for the relative uncertainty in N the sum in quadrature:

$$\frac{\Delta N}{N}=\left[\left[\frac{\sqrt{C}/t}{C/t-C'/t'}\right]^2+\left[\frac{\sqrt{C'}/t'}{C/t-C'/t'}\right]^2+\left[\frac{\Delta I}{I}\right]^2+\left[\frac{\Delta p}{p}\right]^2\right]^{1/2}. \tag{20}$$

The error in the time duration of each measurement is negligible and is not included in the error budget. The uncertainties in the photomultiplier counts C and the background photomultiplier counts C' are both subject to counting statistics and are given by the square root of the accumulated counts. The uncertainty in the number of accumulated current counts resulting from the finite resolution of the digitized signal is negligible.

Several small random errors contribute to the uncertainty in the current measurement. The Keithley electrometer has a temperature coefficients of (0.01% of the reading +0.01% of the scale) per degree K. The temperature in the laboratory fluctuates between 294 and 297 K, which contributes about 0.1% to the random error in the current measurement. Also, the focusing of the electron beam is dependent on the gas pressure. This effect is observed as a change in the current on crp1 and crp2 at different pressures. The current on the first plate, crp1, is lost to the beam before it enters the collision region so that fluctuations in this current are not important. The current on the second plate, crp2, consists of electrons that pass through the electron-atom source and that contribute to the production of radiation but that do not make it to the Faraday cup. The magnitude of the current on crp2 depends on the focusing of the beam and is typically between 0.05% and 0.20% of the Faraday cup current. The resulting systematic offset in the recorded beam current does not affect this measurement and is ignored. However, variations in the current on crp2 caused by fluctuations in the pressure must be accounted for. These variations amount to at most 0.02% of the beam current over the range of pressures used during the measurements. An exception is for the Ne (74.4 nm) line measurement, where, at the highest pressure of 3×10^{-4} Torr, the current on crp2 increases by 0.17% of the Faraday cup current. This small effect is not corrected for but is included in the error budget.

The uncertainty Δp in the pressure is found from propagating the errors through in Eq. (12):

$$\frac{\Delta p}{p}=\left[\left[\frac{\Delta P/t}{P/t-P'/t'}\right]^2+\left[\frac{\Delta P'/t'}{P/t-P'/t'}\right]^2+\left[\frac{\Delta k}{k}\right]^2\right]^{1/2}. \tag{21}$$

Here the quantities P and P' represent the accumulated counts of the digitized pressure signal. The uncertainties ΔP and $\Delta P'$ due to the resolution of these signals is negligible. A small random error in the pressure measurement results from fluctuations in the ionization gauge sensitivity, which cause variations in the ionization gauge calibration constant k, and originate from the variation of the room temperature. Daily calibrations against the spinning rotor gauge indicate that the ionization gauge sensitivity fluctuates within a 1% range. The room-temperature fluctuations also cause small fluctuations in the background pressure in the gas cell. The rate of outgassing from the walls of the gas cell changes slightly with the room temperature and causes an uncertainty in the background pressure signal that is equivalent to 0.1 counts per second. This uncertainty is independent of the pressure of the target gas.

The uncertainty $\Delta A_{2,\mathrm{cal}}$ in Eq. (19) is due to the uncertainty in the absolute calibration of the ionization gauge tube. The value of the fitting parameter A_2 is sensitive to the absolute value of the pressure. A change in the ionization gauge calibration factor k results in a proportional change in the fitted result of the parameter A_2. Two sources of error contribute to the uncertainty in the absolute ionization gauge calibration k. The largest error stems from the uncertainty in the calibration at the National Institute of Standards and Technology of the accommodation coefficient for helium and nitrogen of the SRG rotor. The second uncertainty is introduced in the transfer of the accommodation coefficient to other gases.

D. Error budget

Table II gives an overview of the errors that contribute to the experimental uncertainty in the oscillator strength. In the upper half of the table are listed the signals that are measured to obtain the normalized photomultiplier signal N as a function of the gas pressure. The inverse quadrature sums of these uncertainties, ΔN, are the weights when fitting the transmission function to the data. The range of variation of the uncertainties and the median values are listed in the table. The largest uncertainties occur only during measurements at the lowest target gas pressures. These measurements consequently contribute less to the fit due to their reduced weights. In practice only 10% of the recorded data exhibit an uncertainty of more than 1% in the photon count rate or in the background pressure.

In the lower half of the table the error budget for the final result of the oscillator strength is summarized. The uncertainty in the fitted value of the fitting parameter $\Delta A_{2,\mathrm{fit}}$ depends largely on the quality of the data

TABLE II. Error budget and final uncertainty in the oscillator strength.

Signal	Uncertainty Range	Median	Source
ΔC	0.33–1.5 %	0.8%	Counting statistics
$\Delta C'$	0.03–1.6 %	0.3%	Counting statistics
ΔI	0.1%	0.1%	Electrometer temperature coefficient
ΔI	0.02%	0.02%	Beam focusing (0.17% for Ne 74.4 nm)
$\Delta P'$	0.01–3.4 %	0.09%	Temperature-dependent outgassing
ΔP	0.5%	0.5%	Ionization gauge sensitivity fluctuations
ΔN	0.6–4.8 %	1.0%	Summed in quadrature [Eqs. (20), (21)]
$\Delta A_{2,\mathrm{fit}}$	1.0–2.3 %	1.4%	Fitting
$\Delta A_{2,\mathrm{cal}}$	1.5–1.53 %	1.53%	Absolute pressure calibration
ΔT	0.5–1.0 %	0.5%	Temperature
Δx	1.57%	1.57%	Transmission distance
Δf	2.4–3.3 %	2.6%	Summed in quadrature [Eqs. (18), (19)]

inasmuch as it follows the shape of the transmission curve. In the present work this uncertainty ranges from 1.0% to 2.3% for the different lines measured. To this uncertainty is added (in quadrature) the uncertainty in the absolute calibration of the pressure measurement, the uncertainty in the absolute temperature of the gas, and the uncertainty in the transmission distance. The median value of the overall uncertainty in the resulting oscillator strength is 2.6%.

The contribution from reemission radiation to the detector signal is reduced to negligible proportions by use of the aluminum baffle. The effect of reemitted radiation on the transmission measurements is illustrated in Fig. 4. Here the measured transmission of the helium $2\,^1P$ resonance line at 58.4 nm is shown for data taken with (open circles) and without (solid circles) the baffle in place. The solid line represents the accurately computed transmission, excluding the effects from reemission of absorbed radiation, calculated with Eq. (7) and using the known value of the oscillator strength for this line [14]. The data obtained without the baffle (solid circles) deviate significantly from the correct transmission curve. A fit of the transmission function to these data results in a value of the oscillator strength that is too low. In addition, χ^2 for this fit is unacceptably large because of the poor agreement between the pressure dependence of the experimental data and the actual shape of the theoretical curve.

Data taken with the baffle in place (open circles in Fig. 4), on the other hand, are in excellent agreement with the computed transmission curve to pressures up to 10^2 μTorr, corresponding to a transmission as low as 0.15. In the present work, the effect of reemission is rendered negligible by excluding data with a transmission of less than 0.4 from the analysis.

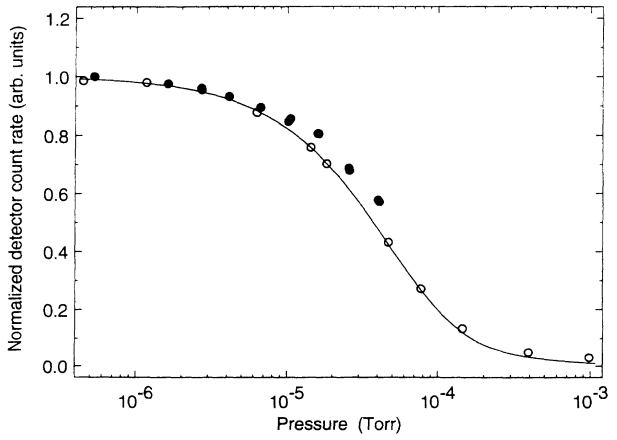

FIG. 4. The transmission function for He 58.4 nm, represented by the solid line, is fitted to the normalized detector count rate $N(p)$(○). The uncertainties in the data are used as weights in the fit. The solid circles (●) are data taken without the reemission baffle and show that in this situation the measured transmission appears to be too large due to reemission of absorbed resonance radiation. A fit of the transmission function to this data results in too small a value of the oscillator strength.

VI. RESULTS

A. Helium

A wavelength scan over the helium emission lines of the $(1snp)\,^1P_1$ Rydberg series at an incident electron energy of 100 eV is shown in Fig. 5. The spectrum is not corrected for absorption of resonance radiation or for the spectral sensitivity of the detector. The He resonance lines at 58.4 nm $(1s2p)$ and 53.7 nm $(1s3p)$ are well isolated from neighboring lines. The lines at 52.5 nm $(1s4p)$ is also resolved but the lines corresponding to higher excitations blend together up to the series limit at 50.5 nm (corresponding to the ionization potential of the helium atom). The spectrometer is set at the central wavelength of the appropriate line shape for the transmission measurements.

During the transmission measurements the width of the exit slit of the spectrometer was 0.07 mm and the temperature of the gas was 303 K. The electron beam current was 1.1×10^{-4} A. The transmission result of the He 58.4-nm resonance line is plotted in Fig. 6. The transmission function is fit to the data using points at pressures below 3×10^{-5} Torr for the 58.4-nm line, and

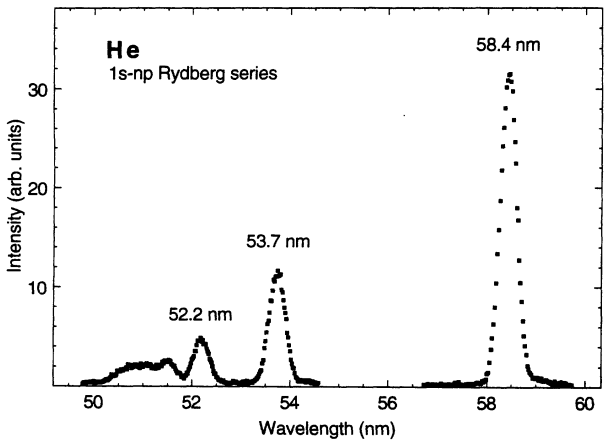

FIG. 5. Wavelength scan for the He lines. The $(1snp)\ ^1P_1$ Rydberg series terminates at 50.5 nm.

at pressures below 1×10^{-4} Torr for the 53.7-nm line. At higher pressures the contribution of secondary (or reemitted) radiation to the detector signal is noticeable [15].

The result for the absorption oscillator strength of the transition from the ground state to the lowest resonance level $(1s2p)\ ^1P_1$ in helium at a wavelength of 58.4 nm is 0.2683±0.0075 (2.8%). The result for the next resonance level $(1s3p)\ ^1P_1$ at a wavelength of 53.7 nm is 0.0717±0.0024 (3.4%).

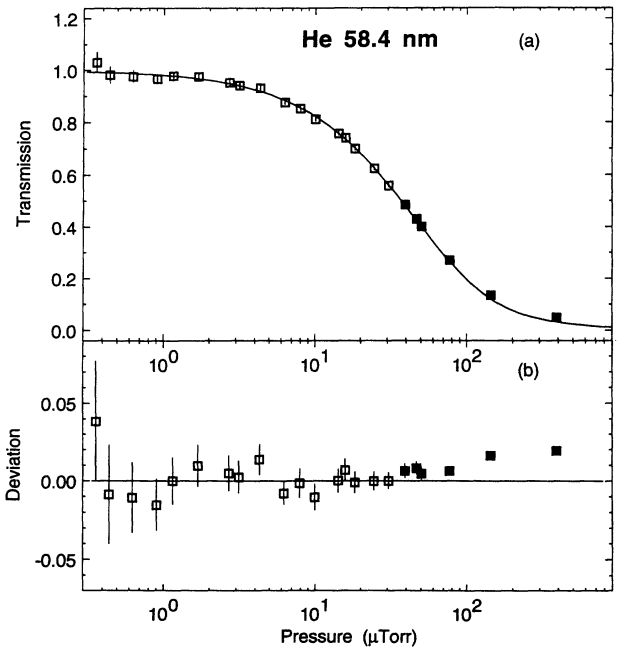

FIG. 6. (a) Transmission of the He 58.4-nm line. (b) Deviation of the He 58.4-nm data points from the fitted transmission curve. □, data included in the fit; ■, data not included in the fit; — — —, fitted curve. The vertical line is the uncertainty due to counting statistics and temperature fluctuations.

B. Neon

The Ne resonance lines at 74.4 and 73.6 nm are separated by only 0.8 nm. The exit slit of the spectrometer was narrowed to 0.025 mm to obtain a better resolution. A wavelength scan over the two lines shows that there is a slight overlap of the wings of the instrumental line profiles. From a Gaussian fit to the spectra it is found that the contribution to the peak intensity of either line from the wing of the other line is less than 1 part in 10 000 and can be neglected. During the measurements the temperature of the gas was 297 K and the electron beam current was 0.83×10^{-4} A.

The oscillator strengths of the Ne 74.4-nm line and the 73.6-nm line are obtained from fitting the transmission function to the data at pressures below 3×10^{-4} and 3×10^{-5} Torr, respectively.

The result for the absorption oscillator strength of the transition from the ground state to the lowest resonance level $(2s^22p^53s)\ ^2P_{3/2}$ in neon at a wavelength of 74.4 nm is 0.010 17±0.000 30 (2.9%), and for the transition to the next resonance level $(2s^22p^53s')\ ^2P_{1/2}$ at a wavelength of 73.6 nm the oscillator strength is 0.1369±0.0035 (2.6%).

C. Argon

The Ar resonance lines at 106.7 and 104.8 nm are free from interference from neighboring lines at an electron impact energy of 60 eV. For the transmission measurements the exit slit width of the spectrometer was set to 0.28 mm. During this series of measurements the heat shield of the electron gun did not make good thermal contact with the holder which contains the cooling water ducts. As a result the temperature of the electron-gun–Faraday-cup assembly (323 K) was somewhat elevated over the temperature of the rest of the gas cell (304 K). The gas temperature near the collision region was 313 K with an uncertainty of 5 K. This uncertainty in the temperature contributes to a somewhat larger uncertainty in the oscillator strength results. The electron beam current was 1.0×10^{-4} A.

Data at argon pressures below 8×10^{-5} Torr are used for the fitting of the transmission function for the 106.7-nm line and data below 7×10^{-6} Torr are used for the 104.8-nm line.

The absorption oscillator strength of the transition from the ground state to the lowest resonance level $(3s^23p^54s)\ ^2P_{3/2}$ in argon at a wavelength of 106.7 nm is 0.0616±0.0021 (3.4%). The result for the next resonance level $(3s^23p^54s')\ ^2P_{1/2}$ at a wavelength of 104.8 nm is 0.2297±0.0093 (4.0%).

D. Krypton

The exit slit was set to the nominal width of 0.07 mm for the transmission measurements of the Kr resonance lines. The temperature of the gas was 300 K during the measurement of the 123.6-nm line and it was 298 K during the measurement of the 116.5-nm line. The electron beam current was 1.1×10^{-4} A.

The spectral scan from 113 to 130 nm shows the pres-

ence of many small background features in addition to the prominent Kr resonance lines. These are identified as second-order Kr II ion lines. Their contribution to the peak of each of the two resonance lines is determined as follows. The first-order Kr II spectrum near 60 nm consists of many lines that appear in unresolved groupings. This spectrum is modeled by fitting multiple Gaussian profiles centered on actual Kr II emission lines [16,17] to these recorded features. The Gaussian line shapes used in the fit are of variable height, but of equal width, corresponding to the width of the instrumental line profile. The second-order Kr II spectrum is generated from the first-order model using the same constant instrumental width for each Gaussian component. The generated second-order spectrum near 120.0 nm is shown in Fig. 7 with the actual recorded spectrum which includes the resonance lines at 116.5 and 123.6 nm. The relative heights and positions of the generated second-order Kr II spectral lines are in excellent agreement with the recorded spectrum surrounding the resonance lines. The contribution from the second-order spectrum to the peak intensity of the resonance lines is found to be 0.33% for both lines. The correction is applied in the analysis of the transmission data and results in an adjustment of the experimental oscillator strength of 0.5%.

Data obtained at pressures below 6×10^{-6} Torr are used in the fitting for the 123.6-nm line and data obtained at pressures below 1×10^{-5} Torr are used for the 116.5-nm line.

The result of the absorption oscillator strength of the transition from the ground state to the lowest resonance level $(4s^24p^55s)\ ^2P_{3/2}$ in krypton at a wavelength of 123.6 nm is 0.1751±0.0049 (2.8%). The result for the next resonance level $(4s^24p^55s')\ ^2P_{1/2}$ at a wavelength of 116.5 nm is 0.1496±0.0038 (2.5%).

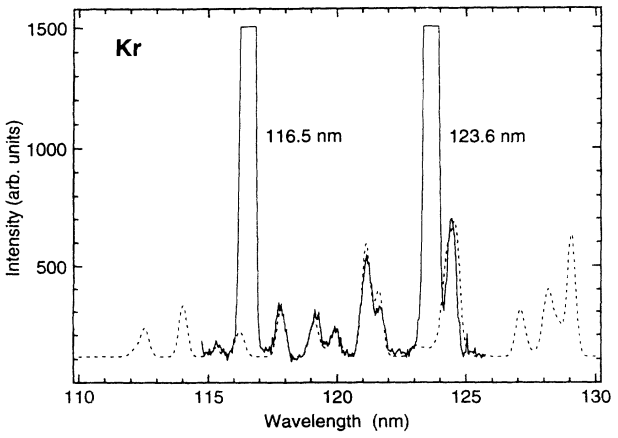

FIG. 7. Fit of the generated second-order spectrum of the Kr II ion lines to the features surrounding the resonance lines. The recorded spectrum is represented by the solid line and the generated second-order spectrum is represented by the dotted line.

VII. DISCUSSION

Experimentally, oscillator strengths have been measured over the past 25 years using a wide variety of techniques. A broad division can be made into (1) optical methods which are based on the detection of radiation and (2) scattering methods in which electrons that are inelastically scattered from the target atom are detected. The optical methods can be further divided into (1) methods that take advantage of the resonant character of resonance transitions, this includes the method used in the present work in which the self-absorption of resonance radiation is measured, (2) spectroscopic studies of the emission or the absorption profile, and (3) lifetime measurements.

The electron scattering methods make use of the observation that at high incident energy and at small scattering angles the projectile electron interacts with the target atom in the same way a resonant photon does. The excitation of an atomic valence electron by a passing energetic electron is characterized by the generalized oscillator strength and is a function of the momentum transfer. In the limit of zero momentum transfer the value of the generalized oscillator strength approaches the optical oscillator strength [18].

Theoretically, the oscillator strength of an absorption or emission line can be expressed in terms of the matrix element of the electric dipole operator between the initial and final states of the transition. The matrix element can be expressed in the length, velocity, or acceleration form [19]. These three formulations are identical when exact wave functions are used. In practice the results differ with the use of approximate wave functions.

The quality of an oscillator strength calculation depends on the accuracy of the wave functions for the states involved and on the validity of the approximations used for the numerical calculations. Since exact wave functions exist only for hydrogenic systems, a number of methods have been developed to obtain useful wave functions for accurate atomic structure calculations. These methods are generally based on the Hartree-Fock self-consistent field approach in which the choice of configurations included and whether electron correlation effects are accounted for may lead to various degrees of sophistication in the calculations.

The assessment of the accuracy of a calculation is usually based on the degree to which the results obtained from using the length, velocity, and acceleration forms agree with one another. It must be noted, however, that agreement between the results from the three forms is a necessary but not a sufficient condition for this accuracy [20]. Additionally the convergence for different numbers of terms included in the expansions of the wave functions is important.

In this section the results of the present absorption oscillator strength measurements are compared to previously reported measurements and calculations. The values of the measured and calculated oscillator strengths are listed by gas species in Tables III through VI.

TABLE III. Helium oscillator strengths. Uncertainties are reported by the author(s). The symbols (l), (v), or (a) indicate a calculation using the length, velocity, or acceleration form of the dipole matrix element, respectively.

Author	Method	He I (58.4) nm $2\ ^1P_1$	He I (53.7 nm) $3\ ^1P_1$
	Experiment		
Present	Absolute self-absorption	0.268 3±0.007 5	0.071 7±0.002 4
W. F. Chan, G. Cooper. and C. E. Brion, Phys. Rev. A **44**, 186 (1991)	Forward electron scattering	0.280±0.014	0.074 1±0.003 7
S. Tsurubuchi, K. Watanabe, and T. Arikawa, J. Phys. B **22**, 2969 (1989)	Absolute self-absorption	0.273±0.008	0.071±0.003
W. B. Westerveld and J. v. Eck, J. Quant. Spectrosc. Radiat. Transfer **17**, 131 (1977); W. B. Westerveld, T. F. A. Mulder, and J. v. Eck, *ibid.* **21**, 533 (1979)	Absolute self-absorption	0.272±0.019[a]	
C. Backx, R. R. Tol, and M. J. van der Weil, J. Phys. B **8**, 2050 (1975)	Forward electron scattering		0.073
J. P. de Jongh and J. van Eck, Physica **51**, 104 (1971)	Relative self-absorption		0.076±0.004
J. M. Burger and A. Lurio, Phys. Rev. A **3**, 64 (1971)	Lifetime: level crossing	0.275±0.007	0.073±0.005
E. N. Lassettre, A. Skerbele, and M. A. Dillon, J. Chem. Phys. **52**, 2797 (1970)	Forward electron scattering	0.269±0.010	
I. Martinson and W. S. Bickel, Phys. Lett. **30A**, 524 (1969)	Lifetime: beam foil	0.27±0.01	
E. S. Fry and W. L. Williams, Phys. Rev. **183**, 81 (1969)	Lifetime: level crossing	0.273±0.011	
R. Lincke and H. R. Griem, Phys. Rev. **143**, 66 (1966)	Plasma: emission profile	0.26±0.07	
F. A. Korolyov and V. I. Odintsov, Opt. Spektrosk. **18**, 968 (1965) [Opt. Spectrosc. (USSR) **18**, 547 (1965)]	Beam: emission profile	0.28±0.02[b] 0.26±0.012[c]	
H. G. Kuhn and J. M. Vaughan, Proc. R. Soc. London, Ser. A **277**, 297 (1964)	Resonance broadening profile	0.377±0.035	
J. Geiger, Z. Phys. **175**, 530 (1963)	Forward electron scattering	0.312±0.04	0.089 8±0.006
	Theory		
J. A. Fernley, K. T. Taylor, and M. J. Seaton, J. Phys. B **30**, 6457 (1987)	Close coupling expansions	0.281 1	0.074 34
C. Froese Fisher, J. Phys. B **7**, L91 (1974)	Hartree-Fock, multiconfiguration	0.275 3 (l) 0.274 4 (v)	
K. R. Devine and A. L. Stewart, J. Phys. B **5**, 2182 (1972)	Hartree-Fock, frozen core	0.274 9 (l) 0.274 7 (v) 0.275 2 (a)	0.073 20 (l) 0.073 16 (v) 0.073 11 (a)
B. Schiff, C. L. Pekeris, and Y. Accad, Phys. A **4**, 885 (1971)	Expansion in perimetric coordinates	0.276 2±0.000 1	0.073±0.001
F. C. Sanders and C. W. Scherr, Phys. Rev. A **181**, 84 (1969)	Variational perturbation	0.276 113 (l) 0.276 182 (v) 0.276 0012 (a)	
A. Dalgarno and E. M. Parkinson, Proc. R. Soc. London, Ser. A **301**, 253 (1967)	Z expansion	0.373	0.113
A. W. Weiss, J. Res. Natl. Bur. Stand. **71A** 163 (1967)	Hylleraas wave function r_{12} explicit	0.275 9 (l) 0.276 1 (v)	0.073 4 (l) 0.073 0 (v)
M. Cohen and P. S. Kelly, Can. J. Phys. **45**, 2079 (1967)	Hartree-Fock, frozen core	0.112	0.032 2
L. C. Green, N. C. Johnson, and E. K. Kolchin, Astrophys. J. **144**, 369 (1966)	Configuration interaction	0.275 37 (l) 0.275 86 (v) 0.269 08 (a)	0.072 92 (l) 0.072 96 (v) 0.070 647 (a)
W. L. Wiese, M. W. Smith, and B. M. Glennon, *Atomic Transition Probabilities: Volume I—Hydrogen through Neon*, NSRDS-NBS 4 (U.S. GPO, Washington, DC, 1966)	Critical compilation	0.276 2	0.073 4

TABLE III. (*Continued.*)

Author	Method	He I (58.4) nm) $2\ ^1P_1$	He I (53.7 nm) $3\ ^1P_1$
B. Schiff and C. L. Pekeris, Phys. Rev. **134**, A638 (1964)	Variational	0.276 16±0.000 01	0.073 4±0.000 1
E. E. Salpeter and M. H. Zaidi, Phys. Rev. **125**, 248 (1962)	Hartree approximation	0.271 7±0.05	0.070 6±0.02
Low and Stewart (unpublished), quoted in A. Dalgarno and A. L. Stewart, Proc. Phys. Soc. London **76**, 49 (1960)	Hylleraas ground-state wave function	0.275	0.074 6
E. Trefftz, A. Schlüter, K. H. Dettmar, and K. Jörgens, Z. Astrophys. **44**, 1 (1957)	Hartree-Fock	0.258 (l)[d] 0.239 (v)[d]	0.070 7 (l)[d] 0.064 6 (v)[d]
W. F. Miller and R. L. Platzman, Proc. Phys. Soc. London, Sect. A **70**, 299 (1957)		0.277	
E. A. Hylleraas, Z. Phys. **106**, 395 (1937)		0.355 5	0.072 20
H. Körwien, Z. Phys. **91**, 1 (1934)		0.295 25	0.078 91
J. A. Wheeler, Phys. Rev. **43**, 258 (1933)		0.266	
J. P. Vinti, Phys. Rev. **42**, 632 (1932)		0.349	0.092 48

[a]The value of 0.262±0.018 in Ref. [4] corrected for thermal transpiration in Ref. [5].
[b]The average value from four emission lines.
[c]The most accurate of the four measurements in footnote b.
[d]Original values by Trefftz corrected by Weiss (1967) for the exact energy.

A. Helium

The simplest of the noble-gas atoms has received much attention. It can be seen in Table III that most of the experimental results are in good agreement with the present results. Only the oldest measurements by Kuhn and Vaughn [21] in 1964, who studied the pressure dependence of the resonance broadening of a visible emission line that has the $2\ ^1P$ level as its lower level and by Geiger [22] in 1963, who measured the angular distribution of 25-keV electrons elastically scattered by helium show a significant deviation from our values. Chan, Cooper, and Brion [23], who used the forward electron scattering method, Tsurubuchi, Watanabe, and Avikawa [24], who also used the method of self-absorption, and Burger and Lurio [25], who did a lifetime measurement employing the zero field level crossing technique quote accuracies for their He 58.4-nm results that are comparable to the present one.

The most accurate theoretical results for the oscillator strengths of the He I 58.4- and 53.7-nm resonance lines are by Schiff, Pekeris, and Accad [14], who used accurate variational wave functions containing from several hundred to up to a thousand terms in the expansions. They quote a precision of ±1 unit in the last digit of their published oscillator strengths, which are 0.2762 for the 58.4-nm line and 0.073 for the 53.7-nm line. They base the evaluation of this uncertainty on the agreement between the results of the calculations using the length, velocity, and acceleration formulations of the dipole matrix element as well as on the convergence of the results for different numbers of terms in the expansions of the wave functions. The present result for the 53.7-nm line in helium is in good agreement with the calculation by Schiff, Pekeris, and Accad [14] and the theoretical result for the 58.4-nm line is just over one standard deviation from the experimental result.

A more recent calculation by Fernley, Taylor, and Seaton [26] resulted in slightly higher values for these oscillator strengths. However, their calculations were not optimized to produce accurate results. Most of the reported calculations after 1957 are in agreement with Schiff's values. The only exceptions are the results from a frozen core Hartree-Fock calculation by Cohen and Kelly [27] and a Z-expansion calculation by Dalgarno and Parkinson [28]. The calculation by Cohen and Kelly produces acceptable values for the oscillator strength of transitions between states in the He isoelectronic sequence, except for the $1s$-np series.

B. Neon

There is a significant spread in the reported experimental and theoretical oscillator strengths for Ne, see Table IV. Only the result by Westerveld, Mulder, and Eck [5], who applied the same technique as the present work, shows good agreement with our result for the 74.4-nm line. Aleksandrov *et al.* [29] and Geiger [30] obtained

TABLE IV. Neon oscillator strengths. (f_1+f_2) indicates that the sum of the oscillator strengths of the two resonance lines is reported, (τ) indicates that the value of the oscillator strength is obtained from a reported lifetime.

Author	Method	Ne I (74.4 nm) $^2P_{3/2}$ (Paschen: $1s_4$)	Ne I (73.6 nm) $^2P_{12}$ (Paschen: $1s_2$)
	Experiment		
Present	Absolute self-absorption	0.010 17±0.000 30	0.136 9±0.003 5
W. F. Chan, G. Cooper, X. Guo, and G. C. Brion, Phys. Rev. A **45**, 1420 (1992)	Forward electron scattering	0.011 8±0.000 6	0.159±0.008
S. Tsurubuchi, K. Watanabe, and T. Arikawa, J. Phys. Soc. Jpn. **59**, 497 (1990)	Absolute self-absorption	0.012 2±0.000 6	0.123±0.006
D. J. Chornay, G. C. King, and S. J. Buckman, J. Phys. B **17**, 3173 (1984)	Lifetime: electron photon coincidence	0.012 1±0.004(τ)	
Y. M. Aleksandrov, P. F. Gruzdev, M. G. Kozlov, A. V. Loginov, V. N. Makhov, R. V. Fedorchuk, and M. N. Yakimenko, Opt. Spektrosk. **54**, 7 (1983) [Opt. Spectrosc. (USSR) **54**, 4 (1983)]	Total absorption	0.012±0.003	0.144±0.024
W. B. Westerveld, T. F. A. Mulder, and J. v. Eck, J. Quant. Spectrosc. Radiat. Transfer **21**, 533 (1979)	Absolute self-absorption	0.010 9±0.000 9	0.147±0.012
C. E. Kuyatt, S. R. Mielczarek, and S. Natali (unpublished), quoted in Ref. [5] as private communication (1977)	Forward electron scattering	0.012±0.001	0.154±0.016
N. D. Bhaskar and A. Lurio, Phys. Rev. A **13**, 1484 (1976)	Lifetime: cascade level crossing	0.012 1±0.000 9(τ)	0.148±0.014(τ)
E. J. Knystautas and R. Drouin, Astron. Astrophys. **37**, 145 (1974)	Lifetime: beam foil	0.007 8±0.000 8	0.161±0.011
D. J. G. Irwin, A. E. Livingston, and J. A. Kernahan, Nucl. Instrum. Methods **110**, 111 (1973)	Lifetime: beam foil		0.158±0.006(τ)
J. P. de Jongh and J. van Eck, Physica **51**, 104 (1971)	Relative self-absorption		0.134±0.010
S. Kazantsev and M. Chaika, Opt. Spektrosk. **31**, 510 (1971) [Opt. Spectrosc. (USSR) **31**, 273 (1971)]	Lifetime: hidden alignment	0.013 8±0.000 8(τ)	
J. A. Kernahan, A. Denis, and R. Drouin, Phys. Scr. **4**, 49 (1971)	Lifetime: beam foil,	0.008 4±0.007(τ)	0.187±0.014(τ)
J. Geiger, Phys. Lett. **33A**, 351 (1970)	Forward electron scattering	0.009±0.002	0.131±0.026
G. M. Lawrence and H. S. Liszt, Phys. Rev. **178**, 122 (1969)	Lifetime: delay coincidence	0.007 8±0.000 4	0.130±0.013
H. G. Kuhn, F. R. S. Lewis, and E. L. Lewis, Proc. R. Soc. London, Ser. A **299**, 423 (1967); E. L. Lewis, Proc. Phys. Soc. London **92**, 817 (1967)	Pressure broadening profile	0.012±0.002	0.168±0.02
F. A. Korolev, V. I. Odintsov, and E. V. Fursova, Opt. Spektrosk. **16**, 555 (1964) [Opt. Spectrosc. (USSR) **16**, 304 (1964)]	Natural broadening profile		0.16±0.014
C. E. Kuyatt and J. A. Simpson, in *Proceedings of the Third International Conference on the Physics of Electronic and Atomic Collisions, London*, 1963, edited by M. R. C. McDowell (North-Holland, Amsterdam, 1964)	Forward electron scattering		0.16(f_1+f_2)
J. Geiger, Z. Phys. **177**, 138 (1964)	Forward electron scattering		0.140±0.01(f_1+f_2)
A. V. Phelps, Phys. Rev. **100**, 1230 (1955) (abstracts of papers presented at the eighth annual Gaseous Electronics Conference)	Imprisonment of resonance radiation	0.012 (τ)	

TABLE IV. (*Continued.*)

Author	Method	Ne I (74.4 nm) $^2P_{3/2}$ (Paschen: $1s_4$)	Ne I (73.6 nm) $^2P_{12}$ (Paschen: $1s_2$)
W. Schütz, Ann. Phys. (Leipzig) **18**, 705 (1933); H. Schillbach, *ibid.* **18**, 721 (1933)	Natural broadening profile		$0.2\pm0.1(\tau)$
	Theory		
M. Y. Amusia, *Atomic Photoeffect* (Plenum, New York, 1990)	Random phase approx. with exchange		0.163 (f_1+f_2)
Y. M. Aleksandrov, P. F. Gruzdev, M. G. Kozlov, A. V. Loginov, V. N. Makhov, R. V. Fedorchuk, and M. N. Yakimenko, Opt. Spektrosk. **54**, 7 (1983) [Opt. Spectrosc. (USSR) **54**, 4 (1983)]	Intermediate coupling	0.0106	0.141
R. F. Stewart, Mol. Phys. **30**, 745 (1975)	Time-dependent Hartree-Fock		0.159
R. Albat and N. Gruen, J. Phys. B **7**, L9 (1974)	Hartree-Fock, many configurations		0.149
P. F. Gruzdev and A. V. Loginov, Opt. Spektrosk. **35**, 3 (1973) [Opt. Spectrosc. (USSR) **35**, 1 (1973)]	Hartree-Fock, many configurations	0.0106 (τ)	0.138 (τ)
M. Aymar, S. Feneuille, and M. Klapisch, Nucl. Instrum. Methods **90**, 137 (1970)	Parametrized potential	0.011 ± 0.001	0.145 ± 0.015
P. F. Gruzdev, Opt. Spektrosk. **22**, 313 (1967) [Opt. Spectrosc. (USSR) **22**, 170 (1967)]	Intermediate coupling	0.035	0.14
W. L. Wiese, M. W. Smith, and B. M. Glennon, *Atomic Transition Probabilities: Volume I—Hydrogen through Neon*, NSRDS-NBS (4) (GPO, Washington, DC, 1966)	Critical compilation	0.0118	0.162
P. S. Kelly, J. Quant. Spectrosc. Radiat. Transfer **4**, 117 (1964)	Hartree-Fock-Slater		0.188 (f_1+f_2)
J. W. Cooper, Phys. Rev. **128**, 681 (1962)	Hartree-Fock		0.163 (f_1+f_2)
A. Gold and R. S. Knox, Phys. Rev. **113**, 834 (1959)	Hartree-Rock *ab initio*	0.011	0.110
	Hartree-Fock semiempirical	0.012	0.121

results that overlap with the present one by virtue of the large uncertainties (25% and 22%, respectively) quoted by these two authors. The theoretical result by Aleksandrov *et al.* [29], on the other hand, agrees very well with our measurement as does the calculation by Gruzdev and Loginov [31] and the calculation by Aymar, Feneuille, and Klapisch [32].

For the 73.6-nm line the experimental results by Aleksandrov *et al.* [29], Westerveld, Mulder, and Eck [5], Blaskar and Lurio [33], de Jongh and van Eck [34], Geiger [30], and Lawrence and Liszt [35] all agree with the present work. The calculations by Aleksandrov *et al.* [29], Gruzdev and Loginov [31], and Aymar, Feneuille, and Klapisch [32] are all in good agreement with our result. The present results for both lines are the most accurate measurements reported.

C. Argon

For Ar the spread in the reported experimental oscillator strengths in Table V is substantial for both argon resonance lines although the results since 1977 show a satisfactory convergence. The results for the 106.7-nm line by Tsurubuchi, Watanabe, and Arikawa [36], Li *et al.* [37], Chornay, King, and Buckman [38], and Westerveld, Mulder, and Eck [5] all overlap with the present result and the measurement by Chan *et al.* [39] just misses our experimental uncertainty. For the 104.8-nm line Tsurubuchi, Watanabe, and Arikawa [36], Li *et al.* [37], Westerveld, Mulder, and Eck [5], and Vallee, Ranson, and Chapelle [40] report overlapping results. The measurement by Chan *et al.* [39] appears to be too high.

TABLE V. Argon oscillator strengths.

Author	Method	Ar I (106.7 nm) $^2P_{3/2}$ (Paschen: $1s_4$)	Ar I (104.8 nm) $^2P_{1/2}$ (Paschen: $1s_2$)
	Experiment		
Present	Absolute self-absorption	0.0616±0.0021	0.2297±0.0093
W. F. Chan, G. Cooper, X. Guo, G. R. Burton, and C. E. Brion, Phys. Rev. A **46**, 149 (1992)	Forward electron scattering	0.0662±0.0033	0.265±0.013
S. Tsurubuchi, K. Watanabe, and T. Arikawa, J. Phys. Soc. Jpn. **59**, 497 (1990)	Absolute self-absorption	0.057±0.003	0.213±0.011
G. P. Li, T. Takayanagi, K. Wakiya, H. Suzuki, T. Ajiro, S. Yagi, S. S. Kano, and H. Takuma, Phys. Rev. A **38**, 1240 (1988)	Forward electron scattering	$0.058^{+0.005}_{-0.008}$	$0.222^{+0.02}_{-0.03}$
D. J. Chornay, G. C. King, and S. J. Buckman, J. Phys. B **17**, 3173 (1984)	Lifetime; electron photon coincidence	0.065±0.005(τ)	
W. B. Westerveld, T. F. A. Mulder, and J. v. Eck, J. Quant. Spectrosc. Radiat. Transfer **21**, 533 (1979)	Absolute self-absorption	0.063±0.005	0.240±0.020
U. Hahn and N. Schwentner, Chem. Phys. **48**, 53 (1980)	Lifetime: synchrontron pulsed source	0.077±0.004(τ)	0.361±0.060(τ)
J. Geiger (unpublished), quoted in Ref. [5] as private communication (1978)	Forward electron scattering	0.066	0.255
C. E. Kuyatt, S. R. Mielczarek, and S. Natali (unpublished), quoted in Ref. [5] as private communication (1977)	Forward electron scattering	0.067±0.007	0.267±0.028
O. Vallee, R. Ranson, and J. Chapelle, J. Quant. Spectrosc. Radiat. Transfer **18**, 327 (1977)	Pressure broadening profile	0.051±0.007	0.210±0.030
G. H. Copley and D. M. Camm. J. Quant. Spectrosc. Radiat. Transfer **14**, 899 (1974)	Pressure broadening profile	0.076±0.008	0.283±0.024
J. W. McConkey and F. G. Donaldson, Can. J. Phys. **51**, 914 (1973)	Electron excitation function	0.096±0.02	
D. J. G. Irwin, A. E. Livingston, and J. A. Kernahan, Nucl. Instrum. Methods **110**, 111 (1973)	Lifetime: beam foil	0.083±0.027	0.35±0.13
J. P. de Jongh and J. van Eck, Physica **51**, 104 (1971)	Relative self-absorption		0.22±0.02
J. Geiger, Phys. Lett. **33A**, 351 (1970)	Forward electron scattering	0.047±0.009	0.186±0.037
R. Burnham and R. C. Isler, Bull. Am. Phys. Soc. **15**, 213 (1970) (minutes of the 36th meeting of the South Eastern Section of the American Physical Society)	Lifetime: level crossing	0.054±0.006(τ)	
G. M. Lawrence, Phys. Rev. **175**, 40 (1968)	Lifetime: delay coincidence	0.059±0.003	0.228±0.021
E. L. Lewis, Proc. Phys. Soc. London **92**, 817 (1967)	Pressure broadening profile	0.063±0.004	0.278±0.02
J. L. Morack and C. E. Fairchild, Phys. Rev. **163**, 125 (1967)	Lifetime: delayed coincidence	0.024±0.002(τ)	
E. Chamberlain, H. G. M. Heideman, J. A. Simpson, and C. E. Kyuatt, in *Abstracts in Proceedings of the Fourth International Conference on the Physics of Electronic and Atomic Collisions Quebec, 1965*, edited by L. Kerwin and W. Fite (Science Bookcrafters, Hastings-on-Hudson, 1968)	Forward electron scattering	0.049	0.181

TABLE V. (*Continued.*)

Author	Method	Ar I (106.7 nm) $^2P_{3/2}$ (Paschen: $1s_4$)	Ar I (104.8 nm) $^2P_{1/2}$ (Paschen: $1s_2$)
G. M. Stacey and J. M. Vaughan, Phys. Lett. **11**, 105 (1964)	Pressure broadening profile	0.036±0.004	0.275±0.02
J. Geiger, Z. Phys. **177**, 138 (1964)	Forward electron scattering		0.233±0.02(f_1+f_2)
	Theory		
M. Y. Amusia, *Atomic Photoeffect* (Plenum, New York, 1990)	Random phase approx. with exchange		0.278 (f_1,f_2)
R. F. Stewart, Mol. Phys. **30**, 745 (1975)	Time-dependent Hartree-Fock		0.27
R. Albat, N. Gruen, and B. Wirsam, J. Phys. B **8**, L82 (1975)	Hartree-Fock, many configurations	0.048	0.188
P. F. Gruzdev and A. V. Loginov, Opt. Spektrosk. **38**, 411 (1975) [Opt. Spectrosc. (USSR) **38**, 234 (1975)]	Hartree-Fock, many configurations	0.061 (τ)	0.231 (τ)
C. M. Lee, Phys. Rev. A **10**, 584 (1974)	Quantum defect	0.059	0.30
C. M. Lee and K. T. Lu, Phys. Rev. A **8**, 1241 (1973)	Quantum defect	0.080	0.21
M. Aymar, S. Feneuille, and M. Klapisch, Nucl. Instrum. Methods **90**, 137 (1970)	Parametrized potential	0.0665±0.0045	0.27±0.02
W. L. Wiese, M. W. Smith, and B. M. Miles, *Atomic Transition Probabilities: Volume II—Sodium through Calcium*, NSRDS-NBS 22 (U.S. GPO, Washington, DC, 1969)	Critical compilation	0.061	0.254
P. F. Gruzdev, Opt. Spektrosk. **22**, 313 (1967) [Opt. Spectrosc (USSR) **22**, 170 (1967)]	Intermediate coupling	0.075	0.15
J. W. Cooper, Phys. Rev. **128**, 681 (1962)	Hartree-Fock		0.33 (f_1+f_2)
R. S. Knox, Phys. Rev. **110**, 375 (1958)	Hartree-Fock, *ab initio*	0.052	0.170

The theoretical calculations of the oscillator strengths of both argon resonance lines also show a large spread. The results by Gruzdev and Loginov [41] in 1975 agree very well with our measurements for both lines as do the first-order velocity results by Aymar, Feneuille, and Klapisch [32]. The present measurements with an uncertainty of 3.4% and 4.0% are the most accurate to date with only Chan *et al.* [39] and Tsurubuchi, Watanabe, and Arikawa [36] reporting comparable uncertainties ranging from 5.0% to 5.3%.

D. Krypton

Again for Kr there is a wide range in the reported experimental and calculated oscillator strength of the krypton resonance lines, see Table VI. The measurements by Geiger [42], Griffin and Hutcherson [43], and Turner [6] are in fair agreement with our result for the 123.6-nm line where Geiger [42] quotes a large uncertainty in his measurement. The calculations by Aymar and co-workers using the velocity form both in 1978 [44] and in 1970 [32] are in agreement with our measured result.

For the 113.6-nm line we find that the experimental result by de Jongh and van Eck [34] and Tsurubuchi, Watanabe, and Arikawa [24,36] agree well with the present result. The calculation by Geiger [42] is also in reasonable agreement with our value while the semiempirical calculation by Dow and Knox [45] is in excellent agreement with our result. The uncertainties in the present measurements are the smallest yet at 2.8% and 2.5% for the 123.6-nm line and the 116.5-nm line, respectively. Matthias *et al.* [46] and Griffin and Hutcherson [43] also quote small uncertainties ranging from 2.9% to 4.7%.

E. Conclusion

The measurements of the oscillator strengths reported here are among the most accurate results found in the literature. The accuracy is due in large part to the application of the spinning rotor gauge for the absolute determination of the gas number density and a careful avoidance of the contribution from secondary radiation (reemission of absorbed radiation) to the detector signal.

TABLE VI. Krypton oscillator strengths.

Author	Method	Kr I (123.6 nm) $^2P_{3/2}$ (Paschen: $1s_4$)	Kr I (116.5 nm) $^2P_{1/2}$ (Paschen: $1s_2$)
	Experiment		
Present	Absolute self-absorption	0.1751±0.0049	0.1496±0.0038
W. F. Chan, G. Cooper, X. Guo, G. R. Burton, and C. E. Brion, Phys. Rev. A **46**, 149 (1992)	Forward electron scattering	0.214±0.011	0.193±0.010
T. Takayanagi, G. P. Li, K. Wakiya, H. Suzuki, T. Ajiro, T. Inaba, S. S. Kano, and H. Takuma, Phys. Rev. A **41**, 5948 (1990)	Forward electron scattering	0.143±0.015	0.127±0.015
S. Tsurubuchi, K. Watanabe, and T. Arikawa, J. Phys. B **22**, 2969 (1989); J. Phys. Soc. Jpn. **59**, 497 (1990)	Absolute self-absorption	0.155±0.011	0.139±0.010
W. F. Ferrell, M. G. Payne, and W. R. Garrett, Phys. Rev. A **35**, 5020 (1987)	Phase matching		0.180±0.027
U. Hahn and N. Schwentner, Chem. Phys. **48**, 53 (1980)	Lifetime: synchrotron pulsed source	0.235±0.019(τ)	0.168±0.027(τ)
J. Geiger, Z. Phys. A **282**, 129 (1977)	Forward electron scattering	0.195±0.039	0.173±0.035
E. Matthias, R. A. Rosenberg, E. D. Poliakoff, M. G. White, S. T. Lee, and D. A. Shirley, Chem. Phys. Lett. **52**, 239(1977)	Lifetime: resonance fluorescence	0.208±0.006	0.197±0.006
J. P. de Jongh and J. van Eck, Physica **51**, 104 (1971)	Relative self-absorption		0.142±0.015
J. Geiger, Phys. Lett. **33A**, 351 (1970)	Forward electron scattering	0.173±0.035	0.173±0.035
P. M. Griffin and J. W. Hutcherson, J. Opt. Soc. Am. **59**, 1607 (1969)	Total absorption	0.187±0.006	0.193±0.009
J. M. Vaughan, Phys. Rev. **166**, 13 (1968)	Resonance broadening profile	0.204±0.02	0.184±0.02
G. I. Chashchina and E. Y. Shreider, Opt. Spektrosk. **22**, 519 (1967) [Opt. Spectrosc. (USSR) **22**, 284 (1967)]	Linear absorption	0.21±0.05	0.21±0.05
E. L. Lewis, Proc. Phys. Soc. London **92**, 817 (1967)	Pressure broadening profile	0.204±0.01	0.184±0.01
J. W. Hutcherson and P. M. Griffin, Bull. Am. Phys. Soc. II **12**, 459 (1967) (abstracts of papers presented at the 1967 Spring Meeting of the American Physical Society)	Total absorption	0.172±0.02	0.189±0.03
R. Turner, Phys. Rev. **140**, A426 (1965)	Lifetime: resonance imprisonment	0.166	
P. G. Wilkinson, J. Quant. Spectrosc. Radiat. Transfer **5**, 503 (1965)	Total absorption	0.158	0.135
J. Geiger, Z. Phys. **177**, 138 (1964)	Forward electron scattering		0.346±0.06(f_1+f_2)
J. Koch, K. Fysiogr. Saellsk. Lund Forerh. **19**, 173 (1949)	Refractive index measurement	0.266	0.266
	Theory		
M. Y. Amusia, *Atomic Photoeffect* (Plenum, New York, 1990)	Random phase approx. with Exchange		0.353(f_1+f_2)
M. Aymar and M. Coulombe, At. Data Nucl. Data Tables **21**, 537 (1978)	Parametrized potential	0.176 (l) 0.193 (v)	0.177 (l) 0.172 (v)
J. Geiger, Z. Phys. A **282**, 129 (1977)	Quantum defect	0.250	0.143
P. F. Gruzdev and A. V. Loginov, Opt. Spektrosk. **38**, 1056 (1975) [Opt. Spectrosc. (USSR) **38**, 611 (1975)]	Hartree-Fock, many configurations	0.190 (τ)	0.177 (τ)
M. Aymar, S. Feneuille, and M. Klapisch, Nucl. Instrum. Methods **90**, 137 (1970)	Parametrized potential	0.19±0.01	0.185±0.005
P. F. Gruzdev, Opt. Spektrosk. **22**, 313 (1967) [Opt. Spectrosc. (USSR) **22**, 170 (1967)]	Intermediate coupling	0.20	0.20

TABLE VI. (*Continued.*)

Author	Method	Kr I (123.6 nm) $^2P_{3/2}$ (Paschen: $1s_4$)	Kr I (116.5 nm) $^2P_{1/2}$ (Paschen: $1s_2$)
J. D. Dow and R. S. Knox, Phys. Rev. **152**, 50 (1966)	Hartree-Fock, *ab initio*	0.138	0.136
	Hartree-Fock, semiempirical	0.152	0.153
J. W. Cooper, Phys. Rev. **128**, 681 (1962)	Hartree-Fock		0.405 (f_1+f_2)

ACKNOWLEDGMENTS

This work was supported in part by NSF Grant No. PHY90-16986 and DOE Contract No. DE-FG05-87ER53259. We gratefully acknowledge the help we received from the Pressure and Temperature Division at the National Institute of Standards and Technology (NIST) in Gaithersburg, MD with the calibration of the Spinning Rotor Gauge.

[1] J. S. Risley and W. B. Westerveld, Appl. Opt. **28**, 389 (1989).
[2] A. McPherson, N. Rouze, W. B. Westerveld, and J. S. Risley, Appl. Opt. **25**, 298 (1986).
[3] A. C. G. Mitchell and M. W. Zemansky, *Resonance Radiation and Excited Atoms* (Cambridge University Press, London, 1934).
[4] W. B. Westerveld and J. V. Eck, J. Quant. Spectrosc. Radiat. Transfer **17**, 131 (1977).
[5] W. B. Westerveld, T. F. A. Mulder, and J. v. Eck, J. Quant, Spectrosc. Radiat. Transfer **21**, 533 (1979).
[6] R. Turner, Phys. Rev. **140**, A426 (1965).
[7] P. W. Erdman and E. C. Zipf, Rev. Sci. Instrum. **53**, 225 (1981).
[8] M. Seya, Sci. Light **2**, 8 (1952).
[9] T. Namioka, J. Opt. Soc. Am. **49**, 951 (1959).
[10] A. F. J. van Raan, J. van der Weg, and J. van Eck, J. Phys. E **5**, 964 (1972).
[11] D. W. Graves, M.S. thesis, North Carolina State University, 1986 (unpublished).
[12] K. E. McCulloogh, S. D. Wood, and C. R. Tilford, J. Vac. Sci. Technol. A **3**, 1738 (1985).
[13] S. Dittman (private communication).
[14] B. Schiff, C. L. Pekeris, and Y. Accad, Phys. Rev. A **4**, 885 (1971).
[15] A complete description of the measurements appears in R. C. G. Ligtenberg, Ph.D. thesis, North Carolina State University, 1992 (unpublished).
[16] A. R. Striganov and N. S. Sventitskii, *Tables of Spectral Lines of Neutral and Ionized Atoms* (IFI/Plenum, New York, 1968).
[17] R. L. Kelly and L. J. Palumbo, *Atomic and Ionic Emission Lines Below 2000 Angstroms—Hydrogen Krypton* (U.S. GPO, Washington, DC, 1973) (NRL Report No. 7599).
[18] E. W. McDaniel, *Atomic Collisions—Electron and Photon Projectiles* (Wiley, New York, 1989).
[19] S. Chandrasekhar, Astrophys. J. **102**, 223 (1945).
[20] C. Froese Fisher, *The Hartree-Fock Method for Atoms* (Wiley, New York, 1977).
[21] H. G. Kuhn and J. W. Vaughan, Proc. R. Soc. London, Ser. A **277**, 297 (1964).
[22] J. Geiger, Z. Phys. **175**, 530 (1963).
[23] W. F. Chan, G. Cooper, and C. E. Brion, Phys. Rev. A **44**, 186 (1991).
[24] S. Tsurubuchi, K. Watanabe, and T. Arikawa, J. Phys. B **22**, 2969 (1989).
[25] J. M. Burger and A. Lurio, Phys. Rev. A **3**, 64 (1971).
[26] J. A. Fernley, K. T. Taylor, and M. J. Seaton, J. Phys. B **20**, 6457 (1987).
[27] M. Cohen and P. S. Kelly, Can. J. Phys. **45**, 2079 (1967).
[28] A. Dalgarno and E. M. Parkinson, Proc. R. Soc. London, Ser. A **301**, 253 (1967).
[29] Y. M. Aleksandrov, P. F. Gruzdev, M. G. Kozlov, A. V. Loginov, V. N. Makhov, R. V. Fedorchuk, and M. N. Yakimenko, Opt. Spektrosk. **54**, 7 (1983) [Opt. Spectrosc. (USSR) **54**, 4 (1983)].
[30] J. Geiger, Phys. Lett. **33A**, 351 (1970).
[31] P. F. Gruzdev and A. V. Loginov, Opt. Spektrosk. **35**, 3 (1973) [Opt. Spectrosc. (USSR) **35**, 1 (1973)].
[32] M. Aymar, S. Feneuille, and M. Klapisch, Nucl. Instrum. Methods **90**, 137 (1970).
[33] N. D. Bhaskar and A. Lurio, Phys. Rev. A **13**, 1484 (1976).
[34] J. P. de Jongh and J. van Eck, Physica **51**, 104 (1971).
[35] G. M. Lawrence and H. S. Liszt, Phys. Rev. **178**, 122 (1969).
[36] S. Tsurubuchi, K. Watanabe, and T. Arikawa, J. Phys. Soc. Jpn. **59**, 497 (1990).
[37] G. P. Li, T. Takayanagi, K. Wakiya, H. Suzuki, T. Ajiro, S. Yagi, S. S. Kano, and H. Takuma, Phys. Rev. A **38**, 1240 (1988).
[38] D. J. Chornay, G. C. King, and S. J. Buckman, J. Phys. B **17**, 3173 (1984).
[39] W. F. Chan, G. Cooper, X. Guo, G. R. Burton, and C. E. Brion, Phys. Rev. A **46**, 149 (1992).
[40] O. Vallee, R. Ranson, and J. Chapelle, J. Quant. Spectrosc. Radiat. Transfer **18**, 327 (1977).
[41] P. F. Gruzdev and A. V. Loginov, Opt. Spektrosk. **38**, 411 (1975) [Opt. Spectrosco. (USSR) **38**, 234 (1975)].
[42] J. Geiger, Z. Phys. A **282**, 129 (1977).
[43] P. M. Griffin and J. W. Hutcherson, J. Opt. Soc. Am. **59**, 1607 (1969).
[44] M. Aymar and M. Coulombe, At. Data Nucl. Data Tables **21**, 537 (1978).
[45] J. D. Dow and R. S. Knox, Phys. Rev. **152**, 50 (1966).
[46] E. Matthias, R. A. Rosenberg, E. D. Poliakoff, M. G. White, S. T. Lee, and D. A. Shirley, Chem. Phys. Lett. **52**, 239 (1977).

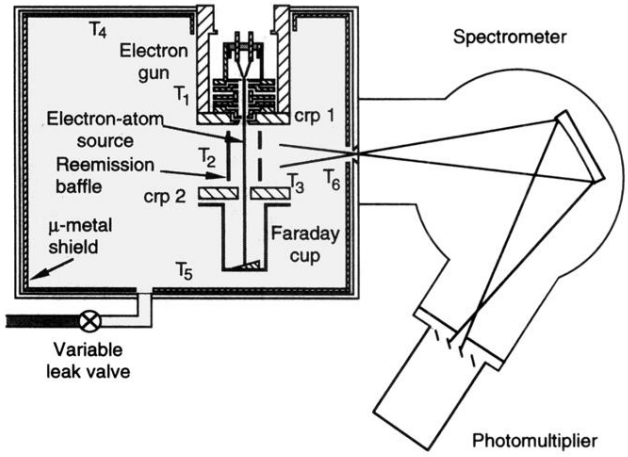

FIG. 1. General overview of the experimental apparatus. The electron beam produced by the electron gun is immersed in the gas and forms the electron-atom source of radiation. An aluminum reemission baffle is inserted between the electron gun and Faraday cup. Light emitted in the direction of the spectrometer is wavelength selected and then detected by the photomultiplier. The μ-metal shield minimizes the penetration of external magnetic fields into the cell. The target gas pressure is regulated with the variable leak valve. The locations of the temperature probes are indicated by T_1 through T_6.